

# Density-Constrained Time-Dependent Hartree-Fock Calculation of $^{16}\text{O}+^{208}\text{Pb}$ Fusion Cross-Sections

A.S. Umar<sup>1a</sup> and V.E. Oberacker<sup>1</sup>

Department of Physics and Astronomy, Vanderbilt University, Nashville, Tennessee 37235, USA

Received: June 14, 2018/ Revised version: date

**Abstract.** We present a fully microscopic study of the  $^{16}\text{O}+^{208}\text{Pb}$  fusion using the density-constrained time-dependent Hartree-Fock theory. The calculated fusion cross-sections are in good agreement with the experimental data for the entire energy range indicating that the incorporation of dynamical effects is crucial in describing heavy-ion fusion.

**PACS.** 21.60.Jz Nuclear Density Functional Theory and extensions – 24.10.Cn Many-body theory

## 1 Introduction

Heavy-ion fusion reactions are a sensitive probe of the size, shape, and structure of atomic nuclei as well as the collision dynamics. Fusion studies using neutron-rich nuclei are becoming increasingly available. Examples include the experiments with heavy neutron-rich  $^{132}\text{Sn}$  beams on  $^{64}\text{Ni}$  [1, 2], and the fusion measurements for the  $^{64}\text{Ni}+^{64}\text{Ni}$  system [3]. What characterized these experiments was the measurement of the fusion cross-sections at very low bombarding energies. Recently, fusion cross-sections for the  $^{16}\text{O}+^{208}\text{Pb}$  system were also measured at extreme sub-barrier energies [4]. Another experimental frontier for fusion is the synthesis of superheavy nuclei in cold and hot fusion reactions [5, 6, 7, 8].

To date quantitative theoretical studies of fusion cross-sections have largely been limited to phenomenological methods, mainly the coupled-channels approach. Specifically, various effects such as neutron transfer [2], compression potential [9], modifications of the inner turning points via the approximate inclusion of neck formation [11, 12], and complex potentials [13] were introduced, in addition to standard channel couplings, to address the recent data at extreme sub-barrier energies. This is surprising since the  $^{16}\text{O}+^{208}\text{Pb}$  system should be an ideal system for coupled-channel calculations. A number of papers have been devoted exclusively to the  $^{16}\text{O}+^{208}\text{Pb}$  system [13, 10]. This underscores the fact that while phenomenological methods provide a useful and productive means for quantifying multitudinous fusion data it is desirable to make contact with the microscopic theories of nuclear structure and reactions.

In the absence of a true many-body theory for calculating sub-barrier fusion all practical calculations are reduced to the calculation of a potential barrier between

the interacting nuclei and a subsequent calculation of tunneling through the barrier. Many of the phenomenological methods use frozen densities for each nuclei and ignore all of the dynamical effects as well as the formation of a neck during the nuclear overlap. It has been demonstrated that for deep sub-barrier energies the inner part of the potential barrier plays a very important role [11, 12]. While the outer part of the barrier is largely determined by the early entrance channel properties of the collision, the inner part of the potential barrier is strongly sensitive to dynamical effects such as particle transfer and neck formation. Recently, an inversion method has been devised [10] to obtain inter-nucleus potentials directly from the fusion data for the  $^{16}\text{O}+^{208}\text{Pb}$  system. In their conclusion the authors propose that dynamical effects, such as neck formation and coordinate dependent mass may be responsible for the modification of the ordinary potentials used in the coupled-channel calculations.

It is generally acknowledged that the time-dependent Hartree-Fock (TDHF) theory provides a useful foundation for a fully microscopic many-body theory of low-energy heavy-ion collisions [14]. The success of the TDHF method is predicated on the expectation that the Pauli principle plays an important role in simultaneously building up a time-dependent mean-field and suppressing the propagation of the strong  $N - N$  interaction terms. With the advent of computer technology it has now become feasible to perform TDHF calculations with no symmetry assumptions regarding the collision process and the effective interaction, and with much more accurate numerical methods [15]. At the same time the quality of effective interactions has also been substantially improved [16]. In this sense, a description of the heavy-ion collisions via the TDHF method may provide a way to incorporate the dynamical effects such as mass transfer and neck formation into the calculation of the ion-ion potential.

<sup>a</sup> e-mail: umar@compisci.cas.vanderbilt.edu

In Section 2 we outline the main features of one such method, the density-constrained TDHF (DC-TDHF) method [17]. The DC-TDHF method was first used to study the fusion reactions of the  $^{64}\text{Ni}+^{132}\text{Sn}$  system [18, 19]. A re-measurement of the lowest energy data point [20] has moved this point exactly onto the DC-TDHF result. We have also performed calculations for the  $^{64}\text{Ni}+^{64}\text{Ni}$  system [21] and showed that an excellent agreement with data is possible. As the DC-TDHF method contains no parameters or normalization its primary success depends on the quality of the description of the ground state properties within the Hartree-Fock framework and the description of the early stages of the ion-ion reaction by the TDHF theory. In this sense we expect the  $^{16}\text{O}+^{208}\text{Pb}$  system to be a good test since most Skyrme parametrizations include these nuclei in the fitting procedure. In Section 2 we also discuss the calculation of ion-ion separation distance, coordinate-dependent mass, and calculation of fusion cross-sections. In Section 3 the calculations for the  $^{16}\text{O}+^{208}\text{Pb}$  system are presented. Final conclusions are given in Section 4.

## 2 Formalism

### 2.1 DC-TDHF method

Recently, we have developed a new method to extract ion-ion interaction potentials directly from the TDHF time-evolution of the nuclear system. In the DC-TDHF approach [17] the TDHF time-evolution takes place with no restrictions. At certain times during the evolution the instantaneous density is used to perform a static Hartree-Fock minimization while holding the neutron and proton densities constrained to be the corresponding instantaneous TDHF densities. In essence, this provides us with the TDHF dynamical path in relation to the multi-dimensional static energy surface of the combined nuclear system. The advantages of this method in comparison to other mean-field based microscopic methods such as the constrained Hartree-Fock (CHF) method are obvious. First, there is no need to introduce artificial constraining operators which assume that the collective motion is confined to the constrained phase space, second the static adiabatic approximation is replaced by the dynamical analogue where the most energetically favorable state is obtained by including sudden rearrangements and the dynamical system does not have to move along the valley of the potential energy surface. In short we have a self-organizing system which selects its evolutionary path by itself following the microscopic dynamics. Some of the effects naturally included in the DC-TDHF calculations are: neck formation, mass exchange, internal excitations, deformation effects to all order, as well as the effect of nuclear alignment for deformed systems. In the DC-TDHF method the ion-ion interaction potential is given by

$$V(R) = E_{\text{DC}}(R) - E_{A_1} - E_{A_2}, \quad (1)$$

where  $E_{\text{DC}}$  is the density-constrained energy at the instantaneous separation  $R(t)$ , while  $E_{A_1}$  and  $E_{A_2}$  are the bind-

ing energies of the two nuclei obtained with the same effective interaction. In writing Eq. (1) we have introduced the concept of an adiabatic reference state for a given TDHF state. The difference between these two energies represents the internal energy. The adiabatic reference state is the one obtained via the density constraint calculation, which is the Slater determinant with lowest energy for the given density with vanishing current and approximates the collective potential energy [22]. We would like to emphasize again that this procedure does not affect the TDHF time-evolution and contains no *free parameters* or *normalization*.

In addition to the ion-ion potential it is also possible to obtain coordinate dependent mass parameters. One can compute the “effective mass”  $M(R)$  using the conservation of energy

$$M(R) = \frac{2[E_{\text{c.m.}} - V(R)]}{\dot{R}^2}, \quad (2)$$

where the collective velocity  $\dot{R}$  is directly obtained from the TDHF evolution and the potential  $V(R)$  from the density constraint calculations.

### 2.2 Calculation of $R$

In practice, TDHF runs are initialized with energies above the Coulomb barrier at some large but finite separation. The two ions are boosted with velocities obtained by assuming that the two nuclei arrive at this initial separation on a Coulomb trajectory. Initially the nuclei are placed such that the point  $x = 0$  in the  $x - z$  plane is the center of mass. During the TDHF dynamics the ion-ion separation distance is obtained by constructing a dividing plane between the two centers and calculating the center of the densities on the left and right halves of this dividing plane. The coordinate  $R$  is the difference between the two centers. The dividing plane is determined by finding the point at which the tails of the two densities intersect each other along the  $x$ -axis. Since the actual mesh used in the TDHF calculations is relatively coarse we use a cubic-spline interpolation to interpolate the profile in the  $x$ -direction and search for a more precise intersection value. This procedure has been recently described in Ref. [23] in great detail. We have confirmed with the authors of Ref. [23] that our  $R$  values are in exact agreement with their calculations for the  $^{16}\text{O}+^{208}\text{Pb}$  system.

The above procedure works well after the formation of the neck between the two ions. However, at some point when the two ions are substantially overlapping the procedure starts to fail. While this does not occur for the  $R$  values used in this calculation, it may be desirable to find an alternate way of determining the  $R$  value. We have found that if one defines the ion-ion separation as  $R = R_0 \sqrt{|Q_{20}|}$ , where  $Q_{20}$  is the mass quadrupole moment for the entire system, calculated by using the collision axis as the symmetry axis, and  $R_0$  is a scale factor determined to give the correct initial separation distance at the start of the calculations. Calculating  $R$  this way

yields almost identical results to the previous procedure until that procedure begins to fail and continues smoothly after that point. We have compared the two methods for the  $^{16}\text{O}+^{16}\text{O}$  system for which the dividing plane is essentially at the origin for all  $R$  values. We find that the quadrupole method gives the correct  $R$  value even after substantial overlap. Of course the minimum value of  $R$  calculated this way is never zero but is determined by the quadrupole moment of the composite system. In this sense the above approach may be useful for fission studies.

### 2.3 Fusion cross-section

We now outline the calculation of the total fusion cross section using an arbitrary coordinate-dependent mass  $M(R)$ . Starting from the classical Lagrange function

$$L(R, \dot{R}) = \frac{1}{2}M(R)\dot{R}^2 - V(R), \quad (3)$$

we obtain the corresponding Hamilton function

$$H(R, P) = \frac{P^2}{2M(R)} + V(R), \quad (4)$$

where the canonical momentum is given by  $P = M(R)\dot{R}$ . Following the standard quantization procedure for the kinetic energy in curvilinear coordinates [25]

$$T = \frac{-\hbar^2}{2} \left[ g^{-\frac{1}{2}} \frac{\partial}{\partial q^\mu} g^{\frac{1}{2}} g^{\mu\nu} \frac{\partial}{\partial q^\nu} \right], \quad (5)$$

where  $g_{\mu\nu}(q)$  denotes the metric tensor and  $g^{\mu\nu}(q)$  the reciprocal tensor, one obtains the quantized Hamiltonian

$$H(R, \hat{P}) = \frac{1}{2} \left[ M(R)^{-\frac{1}{2}} \hat{P} M(R)^{-\frac{1}{2}} \hat{P} \right] + V(R). \quad (6)$$

with the momentum operator  $\hat{P} = -i\hbar d/dR$ . The total fusion cross-section

$$\sigma_f = \frac{\pi}{k^2} \sum_{L=0}^{\infty} (2L+1) T_L, \quad (7)$$

can be obtained by calculating the potential barrier penetrabilities  $T_L$  from the Schrödinger equation for the relative motion coordinate  $R$  using the Hamiltonian (6) with an additional centrifugal potential

$$\left[ H(R, \hat{P}) + \frac{\hbar^2 L(L+1)}{2M(R)R^2} - E_{c.m.} \right] \psi_L(R) = 0. \quad (8)$$

Alternatively, instead of solving the Schrödinger equation with coordinate dependent mass parameter  $M(R)$  for the heavy-ion potential  $V(R)$ , we can instead use the constant reduced mass  $\mu$  and transfer the coordinate-dependence of the mass to a scaled potential  $U(\bar{R})$  using the well known coordinate scale transformation [24]

$$d\bar{R} = \left( \frac{M(R)}{\mu} \right)^{\frac{1}{2}} dR. \quad (9)$$

Integration of Eq. (9) yields

$$\bar{R} = f(R) \iff R = f^{-1}(\bar{R}). \quad (10)$$

As a result of this point transformation, both the classical Hamilton function, Eq. (4), and the corresponding quantum mechanical Hamiltonian, Eq. (6), now assume the form

$$H(\bar{R}, \bar{P}) = \frac{\bar{P}^2}{2\mu} + U(\bar{R}), \quad (11)$$

and the scaled heavy-ion potential is given by the expression

$$U(\bar{R}) = V(R) = V(f^{-1}(\bar{R})). \quad (12)$$

## 3 Results

In our numerical calculations for the  $^{16}\text{O}+^{208}\text{Pb}$  system we have chosen a Cartesian box which is 60 fm along the collision axis and 30 fm in the other two directions. The two nuclei are placed at an initial separation of 24 fm. Calculations are done in 3-D geometry and using the full Skyrme force (SLy4) [16] as described in Ref. [15]. The numerical accuracy of the static binding energies and the deviation from the point Coulomb energy in the initial state of the collision dynamics is on the order of 50 – 150 keV. We have performed density constraint calculations at every 10 fm/c interval or a total of 40 calculations. The accuracy of the density constraint calculations are commensurate with the accuracy of the static calculations.

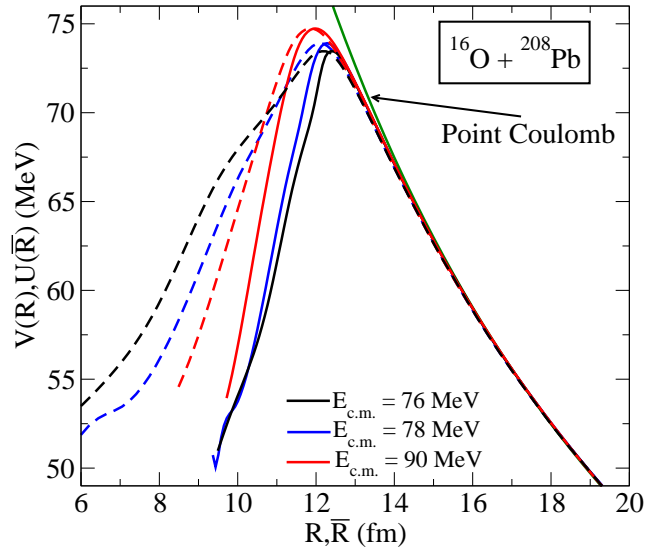


**Fig. 1.** (Colour on-line) Potential barriers,  $V(R)$ , obtained from density constrained TDHF calculations using Eq. (1) at three different energies,  $E_{c.m.} = 76$  MeV (black solid curve),  $E_{c.m.} = 78$  MeV (blue solid curve), and  $E_{c.m.} = 90$  MeV (red solid curve). The three dashed curves correspond to the transformed potential in Eq. (12) using the coordinate dependent masses. Also shown is the point Coulomb potential.

In Fig. 1 we show the ion-ion potentials obtained using Eq. (1) calculated at three different energies,  $E_{c.m.} =$

76 MeV (black solid curve),  $E_{c.m.} = 78$  MeV (blue solid curve), and  $E_{c.m.} = 90$  MeV (red solid curve). The same energy dependence was also observed in the DD-TDHF calculations of Ref. [23] and seems to be more prevalent for heavier systems. For example in  $^{16}\text{O}+^{16}\text{O}$  system we saw a very small energy dependence even though the energy was tripled from 12 MeV to 36 MeV. As can be expected, at lower energies we observe more dynamical effects such as mass transfer, whereas the high energy results seem to approach the frozen-density limit [23]. This is also apparent in the coordinate dependent mass of Eq. (2) shown in Fig. 2 for three different energies,  $E_{c.m.} = 76$  MeV (black solid curve),  $E_{c.m.} = 78$  MeV (blue solid curve), and  $E_{c.m.} = 90$  MeV (red solid curve). The  $R$ -dependence

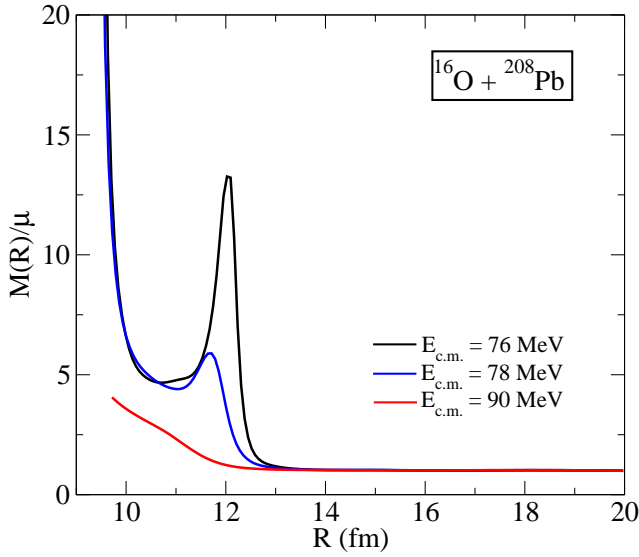


**Fig. 2.** (Colour on-line) Coordinate dependent mass  $M(R)$  scaled by the constant reduced mass  $\mu$ , obtained from Eq. (2), at three different energies,  $E_{c.m.} = 76$  MeV (black solid curve),  $E_{c.m.} = 78$  MeV (blue solid curve), and  $E_{c.m.} = 90$  MeV (red solid curve).

of this mass at lower energies is very similar to the one found in CHF calculations [24]. On the other hand, at higher energies the coordinate dependent mass essentially becomes flat, which is again a sign that most dynamical effects are contained at lower energies. The peak at small  $R$  values is due to the fact that the center-of-mass energy is above the barrier and the denominator of Eq. (2) becomes small due to the slowdown of the ions. We have used the coordinate dependent masses shown in Fig. 2 to obtain the scaled potentials  $U(\bar{R})$  of Eq. (12). These potentials are shown as the dashed curves in Fig. 1. As we see the coordinate dependent mass only changes the inner parts of the barriers for all energies. Furthermore, the effect is largest for the lowest energy collision and diminishes as we increase the collision energy.

We have obtained the fusion cross sections by numerical integration of the Schrödinger equation using the constant reduced mass  $\mu$  and the scaled potential  $U(\bar{R})$ . The fusion barrier penetrabilities  $T_L(E_{c.m.})$  are obtained by

numerical integration of the two-body Schrödinger equation using the *incoming wave boundary condition* (IWBC) method. IWBC assumes that once the minimum of the potential is reached fusion will occur. In practice, the Schrödinger equation is integrated from the potential minimum,  $R_{\min}$ , where only an incoming wave is assumed, to a large asymptotic distance, where it is matched to incoming and outgoing Coulomb wavefunctions. The barrier penetration factor,  $T_L(E_{c.m.})$  is the ratio of the incoming flux at  $R_{\min}$  to the incoming Coulomb flux at large distance. Here, we implement the IWBC method exactly as it is formulated for the coupled-channel code CCFULL described in Ref. [26]. This gives us a consistent way for calculating cross-sections at above and below the barrier energies. The resulting cross-sections are shown in Fig. 3.

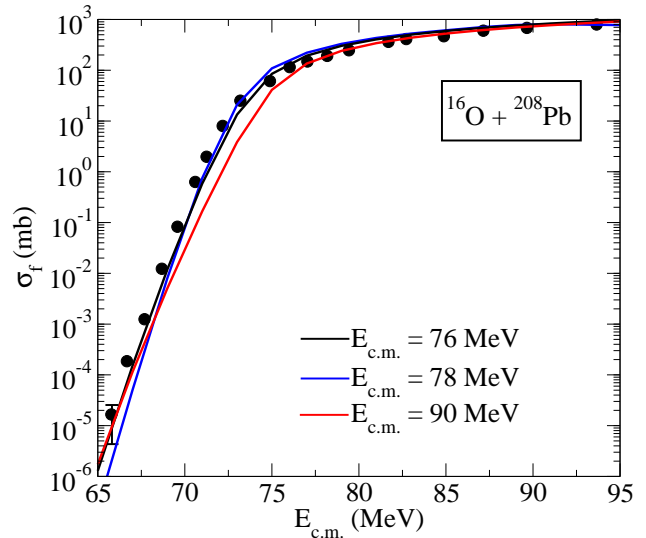


**Fig. 3.** (Colour on-line) Total fusion cross section as a function of  $E_{c.m.}$ . Three separate theoretical cross section calculations are shown, based on the energy-dependent DC-TDHF heavy-ion potentials  $V(R)$  and coordinate dependent masses  $M(R)$  at energies  $E_{c.m.} = 76, 78, 90$  MeV, from which the scaled potentials  $U(\bar{R})$  were obtained. The experimental data (filled circles) are taken from Ref. [4].

We observe that all of the scaled barriers give a very good description of the fusion cross-section at higher energies suggesting these cross-sections are primarily determined by the barrier properties in the vicinity of the barrier peak. Naturally, the extreme sub-barrier cross-sections are influenced by what happens in the inner part of the barrier and here the dynamics and consequently the coordinate dependent mass becomes very important. As we observe in Fig. 3 we get a very good agreement with experiment for the barriers obtained at the lowest two collision energies, whereas the  $E_{c.m.} = 90$  MeV curve underestimates the cross-section at lower energies. Although not shown in Fig. 3 the cross-sections obtained using the unscaled potentials  $V(R)$  and a constant reduced mass  $\mu$  also agree well with the data for  $E_{c.m.} > 77$  MeV but

either significantly over-estimate or under-estimate the cross-section at lower energies.

## 4 Conclusions

In summary, we have used the fully microscopic DC-TDHF method to study  $^{16}\text{O}+^{208}\text{Pb}$  fusion. The standard, parameter free approach of DC-TDHF yields potential barriers that can accurately reproduce the fusion cross-sections. The DC-TDHF approach has now been applied to study a number of systems with very promising results. Our results also agree with the conclusion of Ref. [10] that for the proper description of fusion cross-sections at deep sub-barrier energies the dynamical effects such as neck formation and mass transfer must be included to modify the inner part of the potential barrier. Also, interesting are the implications of the energy dependent barriers as was also discussed extensively in Ref. [23]. These findings underscore the fact that additional modifications needed for phenomenological methods to explain the fusion cross-sections of the  $^{16}\text{O}+^{208}\text{Pb}$  system may largely be due to the inadequacy of the approximations made in treating the nuclear dynamics.

This work has been supported by the U.S. Department of Energy under grant No. DE-FG02-96ER40963 with Vanderbilt University.

## References

1. J. F. Liang *et al.*, Phys. Rev. Lett. **91**, 152701 (2003); **96**, 029903(E) (2006).
2. J. F. Liang *et al.*, Phys. Rev. C **75**, 054607 (2007).
3. C. L. Jiang *et al.*, Phys. Rev. Lett. **93**, 012701 (2004).
4. M. Dasgupta, D. J. Hinde, A. Diaz-Torres, B. Bouriquet, Catherine I. Low, G. J. Milburn, and J. O. Newton, Phys. Rev. Lett. **99**, 192701 (2007).
5. S. Hofmann *et al.*, Eur. Phys. J. **A14**, 147 (2002).
6. Yu. Ts. Oganessian *et al.*, Phys. Rev. C **69**, 021601(R) (2004).
7. W. Loveland, Phys. Rev. C **76**, 014612 (2007).
8. T. Ichikawa, A. Iwamoto, P. Möller, and A.J. Sierk, Phys. Rev. C **71**, 044608 (2005).
9. Ş. Mişicu and H. Esbensen, Phys. Rev. Lett. **96**, 112701 (2006).
10. K. Hagino and Y. Watanabe, Phys. Rev. C **76**, 021601(R) (2007).
11. Takatoshi Ichikawa, Kouichi Hagino, and Akira Iwamoto, Phys. Rev. C **75**, 057603 (2007).
12. Takatoshi Ichikawa, Kouichi Hagino, and Akira Iwamoto, Phys. Rev. C **75**, 064612 (2007).
13. H. Esbensen and Ş. Mişicu, Phys. Rev. C **76**, 054609 (2007).
14. J. W. Negele, Rev. Mod. Phys. **54**, 913 (1982).
15. A. S. Umar and V. E. Oberacker, Phys. Rev. C **73**, 054607 (2006).
16. E. Chabanat, P. Bonche, P. Haensel, J. Meyer and R. Schaeffer, Nucl. Phys. **A635**, 231 (1998); Nucl. Phys. **A643**, 441(E) (1998).
17. A. S. Umar and V. E. Oberacker, Phys. Rev. C **74**, 021601(R) (2006).
18. A. S. Umar and V. E. Oberacker, Phys. Rev. C **74**, 061601(R) (2006).
19. A. S. Umar and V. E. Oberacker, Phys. Rev. C **76**, 014614 (2007).
20. J. F. Liang, D. Shapira, C. J. Gross, R. L. Varner, J. R. Beene, P. E. Mueller, and D. W. Stracener, Phys. Rev. C **78**, 047601 (2008).
21. A. S. Umar and V. E. Oberacker, Phys. Rev. C **77**, 064605 (2008).
22. R. Y. Cusson, P. -G. Reinhard, M. R. Strayer, J. A. Maruhn, and W. Greiner, Z. Phys. A **320**, 475 (1985).
23. Kouhei Washiyama and Denis Lacroix, Phys. Rev. C **78**, 024610 (2008).
24. K. Goeke, F. Grümmer, and P. -G. Reinhard, Ann. Phys. **150**, 504 (1983).
25. M.R. Spiegel, *Vector Analysis*, Schaum's Outline Series, McGraw-Hill (1959).
26. K. Hagino, N. Rowley, and A. T. Kruppa, Comp. Phys. Comm. **123**, 143 (1999).